The Removal of Turbulent Broadening in Radar Doppler Spectra Using Linear Inversion with Double-Sided Constraints

DAVID M. BABB AND JOHANNES VERLINDE

The Pennsylvania State University, University Park, Pennsylvania

BERT W. RUST

National Institute of Standards and Technology, Gaithersburg, Maryland

(Manuscript received 19 August 1999, in final form 11 January 2000)

ABSTRACT

Remote sensing instruments have the ability to collect data over extensive temporal periods and spatial regions. A common thread between all these sensors is the need to relate the measured quantity to a meaningful observation of a system property. If the relationship between each measurement and the set of atmospheric quantities that influence that measurement is known, the problem can be reduced to a set of linear equations. Solving for the unknown atmospheric quantities then becomes a linear algebra problem, where the solution vector is equal to the inverse of the kernel matrix multiplied by the set of independent measurements. However, in most remote sensing applications, inversion of the kernel matrix is unstable, resulting in the amplification of measurement and computational uncertainties. Techniques to circumvent this error amplification have focused on methods of constraining the solution. In this paper, the authors adapt an existing technique to do such an inversion. Noise reduction is accomplished by the addition of double-sided inequality constraints for each unknown variable. The advantage of such a technique is the ability to individually adjust the solution space of each individual unknown, depending on a priori knowledge.

The inversion algorithm is applied to the problem of retrieving radar Doppler spectra, which have been artificially broadened by turbulent air motions. First, to test the algorithm, radar Doppler spectra were simulated using known drop size and vertical air motion distributions. The simulated spectra were used as input to the retrieval algorithm, and the results were compared to the initial quiet-air spectrum. Results indicate that accurate retrievals can be performed despite the addition of moderate amounts of noise to the simulated spectra. Then, to demonstrate the practical retrieval of quiet-air Doppler spectra, the algorithm was used to process radar observations collected from continental stratocumulus. From these retrievals, a two-dimensional map of the large-scale vertical motions within the cloud was constructed as well as a profile of vertical velocity variance. In addition, a drop size distribution was also derived from an updraft region of the cloud.

1. Introduction

Over the last few decades, observation of the earth–atmosphere system has systematically shifted from being primarily in situ based to relying on remote sensing instruments. Remote sensing instruments have the ability to collect data over extensive temporal periods and spatial regions and are inexpensive compared with equivalent amounts of data collected using in situ instruments. A wide range of sensors is used, both ground-based and satellite-borne, and include nearly all available wavelengths, from ultraviolet to microwave. A common thread between all these sensors is the need to relate the measured quantity to a meaningful observation of a system property. Since the measured quantity is frequently related to the system property through a complex (integral) relationship, retrieving the system property is difficult. Despite the range of remote sensing applications, most use a similar methodology for retrieving the system property. In this paper, we present the methodology to do such an inversion and apply it to the inversion of radar-measured Doppler velocity power spectra to obtain the size distribution of cloud hydrometeors.

The problem, in general, may be defined as a mapping from the system-property space into measurement space. The mathematical operator (or kernel function) relating system properties to a measurement assigns weights to all variables in the system-property space such that the measurement represents an integrated measure of the entire system-property space. Typically, more than one type of measurement is taken (i.e., mea-

Corresponding author address: Dr. David M. Babb, Dept. of Meteorology, The Pennsylvania State University, 503 Walker Bldg., University Park, PA 16802-5013.
E-mail: dbabb@essc.psu.edu

surements at different wavelengths), with each measurement having a different operator relating it to the system properties. The retrieval problem is then a problem of inverting the operator to obtain the desired system properties from the measurements (Twomey 1977).

We illustrate the problem further with our specific application of retrieving the size distribution of cloud hydrometeors from radar-measured velocity power spectra. Knowing hydrometeor size distributions of clouds is important for many applications, including studies of the physics of clouds and climate. For example, the Department of Energy has an ongoing, multiyear Atmospheric Radiation Measurement (DOE–ARM) program (Stokes and Schwartz 1994) with the purpose of characterizing the radiative impact of clouds on climate. This radiative impact is strongly related to the hydrometeor size distribution (e.g., Stevens and Webster 1979; Radke et al. 1989).

It has long been suggested that the cloud hydrometeor size distributions may be obtainable from Doppler power spectra collected using a vertically pointing cloud radar (e.g., Rogers and Pilie 1962; Boyenual 1960; Lhermitte 1960). The Doppler spectrum is a measure of received power per unit phase shift. The phase shift in the received power is a result of the beam-parallel motions of all the individual scatters within the illuminated volume. The magnitude of the received power is a function of both the sizes and numbers of drops in each phase shift interval. Therefore, if the motion of the scatters is attributed only to their terminal fall speed and if this fall velocity is a unique function of hydrometeor size, the power spectrum is intimately related to the hydrometeor size distribution.

Unfortunately, this relationship is not straightforward. The measured velocity of any scatterer is the sum of its (quiet air) fall velocity and the ambient air motions. The unknown air motion can be divided into a radar–volume mean and perturbation (volume turbulent) component. The mean wind acts on all scatters equally, thus displacing the entire spectrum along the velocity axis. Conversely, the perturbation component of the vertical wind varies through the extent of the radar volume so that its contribution to any particle's motion will differ throughout the volume. The total effect of the turbulence is then to broaden the quiet-air fall spectrum. This broadening occurs because similarly sized hydrometeors at different locations within the radar volume experience different ambient conditions and hence have different perceived fall velocities.

With this definition of the problem, the hydrometeor size distribution is the desired system property and the Doppler power spectrum is the the measurement. The received power at any given velocity interval consists of power from different sized drops that appear to be falling at the same velocity due to different turbulent contributions. The operator in this case then is the probability of a hydrometeor encountering a particular velocity within the turbulence distribution.

In this paper, we will demonstrate a technique that can be used to remove the effects of the turbulent broadening of Doppler spectra from vertically pointing, 3-mm wavelength cloud radar. This technique characterizes the artificial broadening as a set of linear equations, which are solved using linear algebra. Since the problem is ill-conditioned, the inversion of the coefficient matrix requires constraints. A general approach using double-sided inequality constraints is adapted from Pierce and Rust (1985) and is of a similar form as presented by Rogers (1976). In this algorithm, a double-sided constraint is placed on each of the unknown variables. The width of each constraining interval is independent of surrounding intervals, thus allowing the problem to be tightly constrained in certain regions and loosely constrained in others, depending on the available knowledge about the expected solution.

2. Methodology

Over the years different approaches have been taken into account for the contributions of the radar-volume mean- and turbulent-wind components on profiling-radar measurements.[1] Early studies used radars that were sensitive only to precipitation particles. The first group of these relied on simple estimation of the vertical mean wind contribution and assumed that turbulence broadening was negligible (e.g., Battan 1964; Rogers 1964). Others also assumed negligible turbulent contribution but solved for a two-parameter drop size distribution from several measured moments of the velocity spectrum (e.g., Hauser and Amayenc 1981; Hauser and Amayenc 1983). However, Hauser and Amayenc (1983) concluded that radar volume turbulence could not be ignored because it leads to an overestimation of the shape factor and thus large errors in the retrieved number concentration. Building on this finding, several studies were conducted using a VHF Doppler radar (wavelength $\sim$6.5 m), taking advantage of the ability of these radars to observe clear-air motions directly via Bragg scattering (e.g., Fukao et al. 1985; Wakasugi et al. 1985). Wakasugi et al. (1987) used the clear-air signal to remove the mean wind and also considered the impact of turbulence on the retrievals, thus including all contributions. However, the long wavelength radars usually are not sufficiently sensitive to detect very small hydrometeors and so cannot be used to determine cloud droplet distributions.

Subsequent studies (Gossard 1988; Gossard and Strauch 1989; Gossard et al. 1990; Gossard 1994) fur-

[1] We would like to caution the readers that what we refer to as the radar-volume mean- and turbulent-wind component will vary with the radar (i.e., beamwidth) and processing (i.e., time required to collect samples). Thus, a precipitation radar with a 1° beamwidth will sample a column with diameter on the order of hundreds of meters, compared with tens of meters for a cloud radar (beamwidth 0.17°).

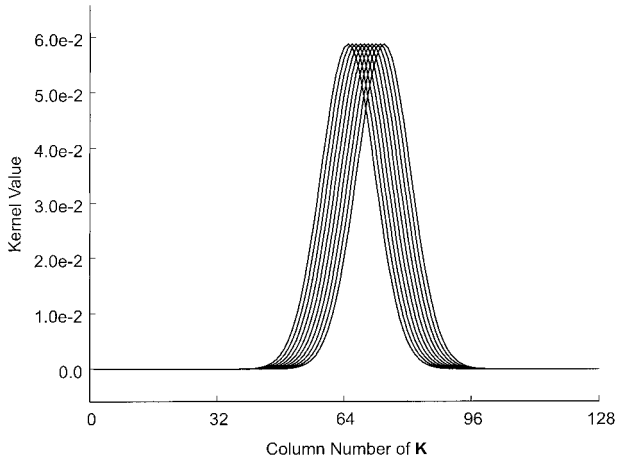

FIG. 1. Plot of rows 64 through 74 of a kernel matrix having a dimension of 128. The value of w_σ for this kernel is 0.3 m s^{-1}.

ther improved the technique presented by Wakasugi by using a shorter wavelength radar (~0.33 m). However, Gossard commented that the retrieved distributions are more representative of drizzle than cloud drops. He noted that the clear-air return contaminated the cloud spectral peak and suggested that a millimeter-wave radar would be better suited because the droplet backscatter far exceeds the clear-air return. In a more recent study, Gossard et al. (1997) applied their drop distribution retrieval method using a 35-GHz radar (8-mm wavelength). They show reasonable retrievals of cloud and drizzle drop distributions from marine stratocumulus. Unfortunately, there are no in situ observations for comparison.

Babb et al. (1999) applies Gossard's technique to continental stratus cloud observations with collocated aircraft observations. They show good agreement between the retrieved and aircraft-observed distributions. However, the algorithm relies on two restrictive assumptions, and a different approach is necessary in order to provide a more robust retrieval technique. Both Gossard et al. (1997) and Babb et al. (1999) parameterized the drop size distribution as a single-mode gamma function. While a single-mode gamma or lognormal drop size distribution is a good approximation for liquid clouds when the sample volume is sufficiently large (Miles et al. 2000), radar is particularly sensitive to large hydrometeors, the presence of which has a negligible impact on such fitted distributions. Small deviations in the large particle tail of the analytical distribution will contribute disproportionately to the measured signal, resulting in skewed retrievals. Second, in both studies, it was assumed that all hydrometeors are liquid drops. However, many clouds are either mixed phase or all ice, and it is difficult to determine the cloud's phase from the measurements. These assumptions are made *before* the turbulence is removed so that any violations in the assumptions about the drop distribution affect the removal of the turbulent broadening.

Optimally, one seeks to remove the effects of turbulent broadening without making any assumptions about the hydrometeors. The result of such a technique would be the (quiet air) fall velocity spectrum of the hydrometeors, shifted along the velocity axis by the value of the volume-mean vertical wind. Since the cloud radar can detect those very small cloud drops that have negligible terminal fall velocity, the mean vertical velocity can be determined by realizing that it corresponds to the retrieved velocity of the smallest drops. After all background air motions are removed, the drop size distribution can be retrieved from the quiet-air spectrum. Although assumptions concerning the characteristics (phase, crystal habit, etc.) of the cloud particles still have to be made, these assumptions do not affect the removal of the air motions. Moreover, determining the cloud particle characteristics will be easier given spectra from which the turbulence contamination has been removed because populations of different hydrometeor classes will tend to have distinctly different fall velocity spectra.

Gossard and Strauch (1989) proposed such a technique using both an iterative method and a Fourier decomposition technique. However, the turbulence broadening effect is a smoothly varying function in velocity space. It is well known that problems with smooth weighting functions present mathematical and numerical difficulties that lead to solutions that are generally unstable (Twomey 1977). For such problems, methods have been developed in many disciplines to contain these numerical instabilities (e.g., Rust and O'Leary 1994; Rust 1998; Twomey 1977; Rogers 1976; Dubovik et al. 1995). These methods have mainly focused on the incorporation of information about the expected solution into the problem, thus improving the likelihood of obtaining a correct solution. The challenge is to sufficiently improve the solution without forcing the solution to a particular value.

We begin the explanation of the technique with a restatement of the problem in a mathematical format. The model of spectral broadening presented in Gossard (1988) and subsequent papers is given by

$$S_{\text{meas}}(x_i)\Delta x = \int_{-\infty}^{0} S_Q(x_j)K(x_j - x_i)\, dx_j, \qquad (1)$$

where $S_{\text{meas}}(x_i)\Delta x$ is the measured spectral reflectivity at the ith velocity bin (having width Δx) and $S_Q(x_j)dx_j$ is the quiet-air spectral reflectivity at the ith velocity bin. The limits of integration are limited to $[0, -\infty)$ because there are no quiet-air drops with upward velocities $\{S_Q(x) = 0 \,|\, x > 0\}$. The function K consists of the weighting values applied to the spectral reflectivity values of neighboring velocity bins and represents the smearing effects of the turbulence. Since the functional form of K is the same for any value of i (just shifted along the x_j axis), the integrand is formally known as the *convolution product*, and Eq. (1) is referred to as a

Fredholm integral of the first kind. Henceforth, we will refer to the function K as the *kernel function* or simply *kernel*.

The kernel function K represents the turbulence probability density function (PDF) (i.e., the probability of a given turbulent air motion causing a particle to appear to be falling at the same speed as the particles of interest, which are of a different size). We choose a Gaussian function of the form

$$K(x_j - x_i) = \frac{1}{\sqrt{\pi} w_\sigma} \exp\left[-\left(\frac{x_j - x_i}{w_\sigma}\right)^2\right], \qquad (2)$$

where w_σ is the width of the distribution and represents the turbulent intensity. However, a kernel function of any form may be selected based on the science of the application.

The integral in Eq. (1) can be approximated using a simple quadrature scheme by dividing the range of $x_j \in (0, -x_{\min})$ into M finite subintervals. The value of $-x_{\min}$ represents the largest negative velocity bin for which observations exist. This leads to an approximation of Eq. (1) given by

$$S_{\text{meas}}(x_i)\Delta x = \sum_{j=1}^{M} S_Q(x_j) K(x_j - x_i)\Delta x_j. \qquad (3)$$

At each velocity bin (representing one measurement) of the observed spectrum $\{x_i | i \in (1, N)\}$, there is a corresponding equation that relates the observed spectral reflectivity $S_{\text{meas}}(x_i)$ to the quiet-air spectrum. If there are N measurements of spectral reflectivity (i.e., an N-point spectrum), then there exists a set of N equations and M unknowns of the following form:

$$\begin{aligned}
S_{\text{meas}}(x_1)\Delta x &= S_Q(x_1)K(x_1 - x_1)\Delta x_1 + S_Q(x_2)K(x_2 - x_1)\Delta x_2 + \cdots + S_Q(x_M)K(x_M - x_1)\Delta x_M,\\
S_{\text{meas}}(x_2)\Delta x &= S_Q(x_1)K(x_1 - x_2)\Delta x_1 + S_Q(x_2)K(x_2 - x_2)\Delta x_2 + \cdots + S_Q(x_M)K(x_M - x_2)\Delta x_M,\\
&\vdots \qquad\qquad \vdots \qquad\qquad \vdots \qquad\qquad \cdots \qquad\qquad \vdots\\
S_{\text{meas}}(x_N)\Delta x &= S_Q(x_1)K(x_1 - x_N)\Delta x_1 + S_Q(x_2)K(x_2 - x_N)\Delta x_2 + \cdots + S_Q(x_M)K(x_M - x_N)\Delta x_M. \qquad (4)
\end{aligned}$$

In order to simplify the derivation, we will make two assumptions, neither of which is critical. Assuming that $\{\Delta x_j = \Delta x | j \in (1, M)\}$ (i.e., the velocity bin width in our solution space is constant), the kernel functions can be reduced to $K(x_j - x_i)\Delta x$. The set of equations can then be rewritten in matrix form as

$$\mathbf{S}_{\text{meas}} = \mathbf{K} \cdot \mathbf{S}_Q, \qquad (5)$$

where $\mathbf{S}_{\text{meas}}$ is an N-column vector, $\mathbf{S}_Q$ is an M-column vector, and $\mathbf{K}$ is an $N \times M$ matrix whose elements are $\mathbf{K}_{i,j} = K(x_j - x_i)\Delta x$. Also, we will assume that $M = N$ in the examples described later, although we assume only that $N \geq M$ for the following theoretical development.

Since the elements of $\mathbf{S}_{\text{meas}}$ contain random measurement errors, one cannot solve Eq. (5) exactly, but from linear algebra, we know the least squares solution is

$$\mathbf{S}_Q = (\mathbf{K}^{\mathrm{T}}\mathbf{E}^{-2}\mathbf{K})^{-1}\mathbf{K}^{\mathrm{T}}\mathbf{E}^{-2} \cdot \mathbf{S}_{\text{meas}}, \qquad (6)$$

where $\mathbf{K}^{\mathrm{T}}$ is the transpose of matrix $\mathbf{K}$, the "-1" is the inverse operator, and $\mathbf{E}^{-2}$ is the inverse of the matrix $\mathbf{E}^2$, which is the variance matrix for the stochastic error in $\mathbf{S}_{\text{meas}}$ (e.g., Pierce and Rust 1985). We assume that these errors are stochastically independent so both $\mathbf{E}^2$ and $\mathbf{E}^{-2}$ are diagonal matrices. Thus, the diagonal elements of $\mathbf{E}^{-2}$ act as inverse weightings to damp the measurements with larger uncertainties. In our application, we assume that all the points on the spectrum have equal error variances, so $\mathbf{E}^2$ becomes a scalar multiple of the identity matrix. It is not necessary to know the exact value of that scalar, since it cancels out in Eq. (6).

The calculation of $\mathbf{S}_Q$ from Eq. (6) appears to be quite straightforward, but for most remote sensing problems, this solution is numerically unstable because of the properties of the kernel matrix $\mathbf{K}$. Figure 1 shows the kernel values for rows 64 through 74 for a $\mathbf{K}$ of dimension 128 and a w_σ of 0.3 m s^{-1}. Since the same turbulence affects each spectral line in a similar manner, each row of the kernel is simply a translation of the turbulence PDF in the column space of $\mathbf{K}$. The result of such row similarity is that any two consecutive rows of the kernel will be nearly linear combinations of each other in a limited precision (computer) environment.

Problems requiring inversions of such near-singular matrices are numerous, and much effort in mathematical and other disciplines has been dedicated to developing techniques to overcome the difficulties outlined above. One avenue of study has been the incorporation of constraints, based on a priori knowledge of what the solution should be, into the inversion process. There are several types of constraints that can be used. If a quantity related to the set of equations is known or can be measured, that quantity can be directly incorporated into the equation set, eliminating one unknown variable, or a new independent equation can be formulated, relating the measured quantity to the existing unknown variables. Both of these procedures decrease the degree of near-singularity of the matrix.

If a general single-bounding characteristic is known

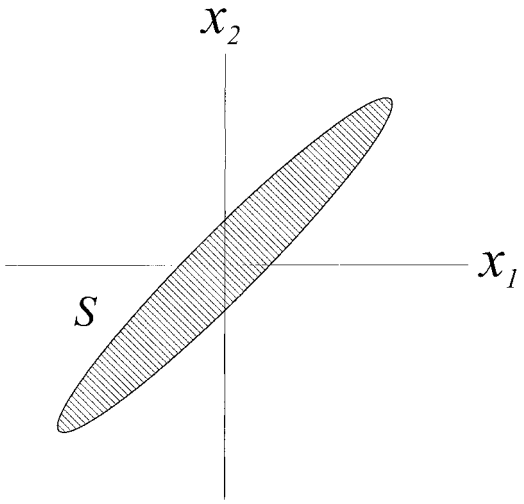

FIG. 2. A two-dimensional example of a solution's confidence ellipsoid for an ill-posed problem. The shaded region represents the solution space.

about the solution set, such as nonnegativity, a one-sided inequality constraint can be applied. This technique involves some sort of iteration-evaluation procedure such as a standard nonnegative least squares (NNLS) algorithm (Lawson and Hanson 1974). If both the upper- and lower-bounding characteristics of a solution are known, then a two-sided inequality constraint is applied. Application of this type of constraint is known by the general term of quadratic programming (e.g., Boot 1964). However, quadratic programming is computationally intensive and is unfeasible for our application. Instead, we will use a suboptimal variant presented by Pierce and Rust (1985) and follow a similar approach to that of Rogers (1976). We will illustrate this technique graphically using a two-dimensional example.

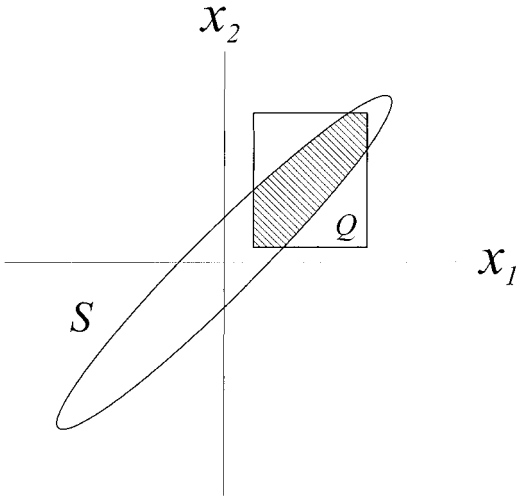

FIG. 3. Upper and lower bounds are used to constrain the solution, which now resides within the intersection of the Q box and the ellipsoid.

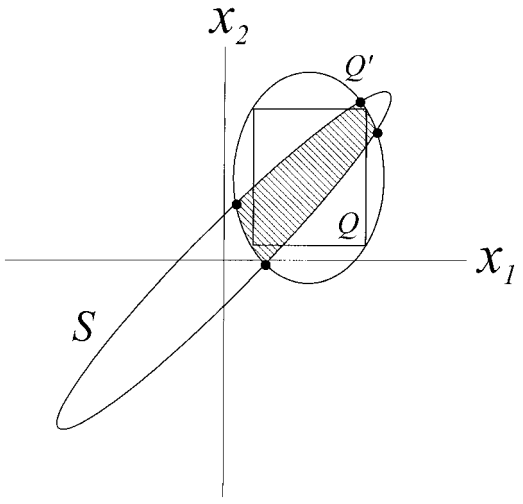

FIG. 4. The Q box is approximated by a circumscribing ellipsoid (Q′). The intersection of the two ellipsoids is more readily solved. Although the solution space is allowed outside of the Q box in this optimization, a majority is still located within the constraints.

Consider an arbitrary M-dimensional confidence ellipsoid (S) for the least squares solution given by Eq. (6). Since $\mathbf{K}$ is ill-conditioned, this S ellipsoid is greatly elongated in the directions of the eigenvectors corresponding to small eigenvalues of $\mathbf{K}^T\mathbf{E}^{-2}\mathbf{K}$ (Fig. 2). The elongated ellipsoid and hence large solution space produces results that are far from the true solution. We seek to improve on the bounds of the S ellipsoid by incorporating knowledge about where the true solution resides.

The bounding of the S ellipsoid is accomplished by adding an N-dimensional bounding box (Q), where the true solution (Fig. 3) is thought to reside. Therefore, each unknown variable x_i is constrained by $p_i \le x_i \le q_i$, where p_i and q_i are the lower and upper bounds on x_i, respectively. Pertinent to our derivation, we define two quantities,

$$\mathbf{d} = \left(\frac{p_1 + q_1}{2}, \frac{p_2 + q_2}{2}, \ldots, \frac{p_n + q_n}{2}\right)^T \quad \text{and}$$

$$\mathbf{Q} = \text{diag}\left(\frac{q_1 - p_1}{2}, \frac{q_2 - p_2}{2}, \ldots, \frac{q_n - p_n}{2}\right), \qquad (7)$$

where $\mathbf{d}$ is a column vector describing the center of the Q box and $\mathbf{Q}$ is a diagonal matrix that contains the widths of the Q box in each dimension. Since the calculation of the solution cannot easily be performed using the intersection of the Q box and S ellipsoid, the Q box is first approximated by a circumscribing ellipsoid, Q′ (Fig. 4). This step does not simplify the calculation enough, so a further suboptimizing step is applied by forming a new ellipsoid (P) as a convex linear combination of the S ellipsoid and Q′ ellipsoid (Fig. 5).

This ellipsoid (P), for which the new solution ($\mathbf{x}$) is computed, has the form

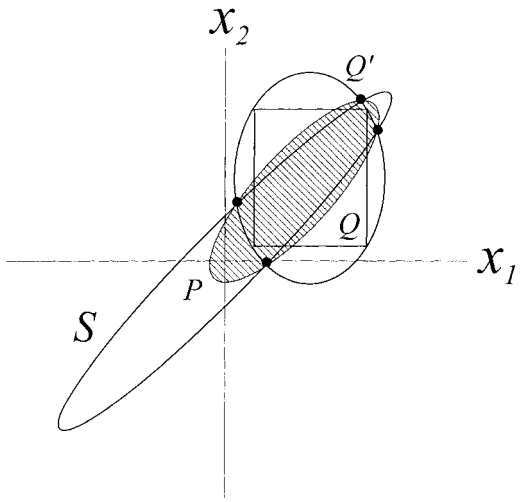

FIG. 5. A new solution space (P) is defined by the convex combination of the two ellipsoids. A weighting function (τ) is used to determine how much contribution from the Q′ ellipsoid is applied in the combination.

$$(\mathbf{Ax} - \mathbf{p})^{\mathrm{T}} \begin{pmatrix} \mathbf{E}^{-2} & 0 \\ 0 & \dfrac{\tau}{M}\mathbf{Q}^{-2} \end{pmatrix} (\mathbf{Ax} - \mathbf{p}) \leq 1, \qquad (8a)$$

with

$$\mathbf{A} = \begin{pmatrix} \mathbf{K} \\ \mathbf{I} \end{pmatrix}, \qquad \mathbf{p} = \begin{pmatrix} \mathbf{S}_{\mathrm{meas}} \\ \mathbf{d} \end{pmatrix}, \qquad (8b)$$

where M is the dimension of $\mathbf{Q}^{-2}$ and τ is a nonnegative weighting constant that describes how much of the Q′ ellipsoid is taken in the convex linear combination. The variable τ is chosen such that the constraint envelope (i.e., the Q′ ellipsoid) affects the solution but does not overwhelm the solution.

The least squares solution vector corresponding to Eqs. (8a) and (8b) is given by

$$\mathbf{S}_Q = \left[\mathbf{K}^{\mathrm{T}}\mathbf{E}^{-2}\mathbf{K} + \frac{\tau}{M}\mathbf{Q}^{-2}\right]\left[\mathbf{K}^{\mathrm{T}}\mathbf{E}^{-2}\mathbf{S}_{\mathrm{meas}} + \frac{\tau}{M}\mathbf{Q}^{-2}\mathbf{d}\right]. \qquad (9)$$

The solution, which is the same as that derived by Rogers (1976), appears to have a form similar to several other constrained inversion techniques but behaves quite differently. Of particularly close resemblance is the inclusion of a bias function to constrain the inversion [e.g., Towmey 1977, Eq. (6.5)]. This solution resembles Eq. (9) with the exception that the term $(\tau/M)\mathbf{Q}^{-2}$ is replaced by $\gamma\mathbf{I}$. In the language of the above graphical derivation, this approach is fixing the width of every dimension of the multidimensional bounding box and using the center of that box (the vector $\mathbf{d}$) to represent the bias vector. If this is the case, $\mathbf{Q}^{-2}$ becomes $\varepsilon\mathbf{I}$ where ε is the uniform width of the Q box. It is easy to see that the γ in Twomey's formulization is now $\tau\varepsilon/M$, which is the weight given to the constraining parameters.

The drawback to this approach is that the resulting constraint envelope resembles a strip surrounding the bias function (Dubovik et al. 1995). Furthermore, Dubovik et al. point out that such a technique prohibits the proper inclusion of a priori information about nonnegativity because to properly do so requires the individual bounds on each unknown to be different, not simply $[d_i + 2\varepsilon; d_i - 2\varepsilon]$. Dubovik et al. circumvent this limitation specifying the solution in logarithmic coordinates. However, we found that performing the inversion using $\log(\mathbf{S}_Q)$ produced unfavorable results. In addition, we find that use of uniform constraint bounds does not allow for a specific enough envelope to be constructed around the expected solution.

In order to see exactly the effects of adding constraints to the kernel matrix, we found it useful to compare the orthogonal decompositions of the two matrices to be inverted, namely $(\mathbf{K}^{\mathrm{T}}\mathbf{E}^{-2}\mathbf{K})$ and $(\mathbf{K}^{\mathrm{T}}\mathbf{E}^{-2}\mathbf{K} + (\tau/M)\mathbf{Q}^{-2})$. Of the many available orthogonal decompositions (e.g., see Lawson and Hanson 1974), we will use singular value decomposition (SVD) because of its usefulness in analyzing the effects of data errors on solutions to the least squares problems. In SVD, the matrix of interest is decomposed into the form $\mathbf{A} = \mathbf{U}\mathbf{\Sigma}\mathbf{V}^{\mathrm{T}}$, where $\mathbf{U}$ and $\mathbf{V}$ are orthogonal matrices and $\mathbf{\Sigma}$ is a diagonal matrix containing the singular values (σ_1, σ_2, . . . , σ_N) of $\mathbf{A}$. If $\mathbf{A}$ is square (as in our application), all of the matrices of the decomposition are also square. Furthermore, their inverses are trivial to compute: $\mathbf{U}$ and $\mathbf{V}$ are orthogonal, so their inverses are equal to their transposes; $\mathbf{\Sigma}$ is diagonal, so its inverse is also a diagonal matrix containing the reciprocals of its elements ($1/\sigma_1$, $1/\sigma_2$, . . . , $1/\sigma_N$); therefore it follows that $\mathbf{A}^{-1} = \mathbf{V}\mathbf{\Sigma}^{-1}\mathbf{U}^{\mathrm{T}}$. At this point, it is obvious where problems in computing $\mathbf{A}^{-1}$ can occur. If a singular value is zero or even very small, then its reciprocal will be very large and will cause its corresponding orthogonal vector in $\mathbf{U}^{\mathrm{T}}$ to dominate the solution. Therefore, by examining the singular values, it is possible to determine a priori the problem components within the solution.

Figure 6 shows a plot of the singular values for the matrices $(\mathbf{K}^{\mathrm{T}}\mathbf{E}^{-2}\mathbf{K})$ and $(\mathbf{K}^{\mathrm{T}}\mathbf{E}^{-2}\mathbf{K} + (\tau/M)\mathbf{Q}^{-2})$ using $N = 128$, $\Delta x = 0.0312$ m s^{-1}, $w_\sigma = 0.3$ m s^{-1}, and a $\mathbf{Q}$ matrix found to work well for our application. Focusing first on the set of singular values corresponding to $\mathbf{K}^{\mathrm{T}}\mathbf{E}^{-2}\mathbf{K}$, we note that no singular values are exactly zero; however, the higher-order singular values ($\sigma_i | \sim 45 < i \leq N$) are extremely small ($\sim 10^{-18}$) and appear to have an asymptotic characteristic. Generally, it is thought that these singular values should in fact be zero (indicating a rank deficient matrix) but have been corrupted by rounding errors into small nonzero quantities (thus the asymptote). The standard approach to inverting matrices with such singular value profiles is to eliminate contributions of the orthogonal vectors corresponding to the very small singular values. This can be accomplished by truncating values below a particular threshold based on measurement noise and the degree of singu-

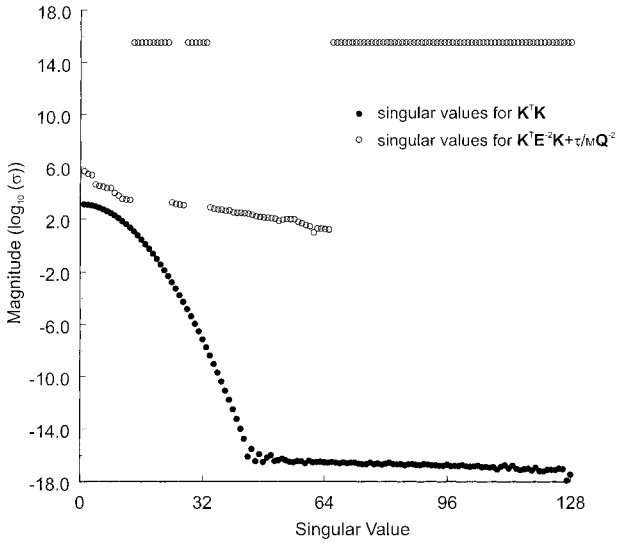

FIG. 6. Plot of the singular values for an unconstrained (solid circles) and a constrained (open circles) kernel. Since the inverse of the kernel depends on the reciprocals of the singular values, errors are generated when singular values are very near zero.

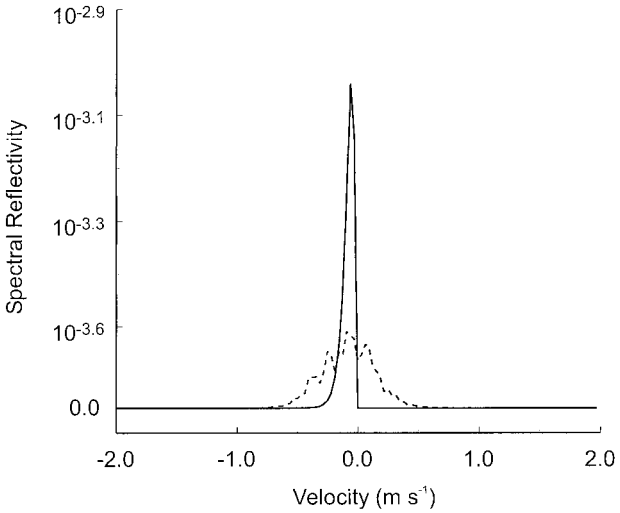

FIG. 8. Numerically simulated quiet-air (solid line) and broadened spectrum (dashed line) for a single cloud-mode drop distribution. The value of w_σ for the turbulent kernel is 0.3 m s^{-1}.

larity of the kernel (e.g., Golub and Kahan 1965). In our application, however, this truncation approach eliminates the higher-frequency components of the solution vector resulting in an estimate that is not only overly smoothed, but also contains erroneous oscillations.

In contrast, the singular values of the constrained matrix ($\mathbf{K}^T\mathbf{E}^{-2}\mathbf{K} + (\tau/M)\mathbf{Q}^{-2}$) are much improved from those of $\mathbf{K}^T\mathbf{E}^{-2}\mathbf{K}$. Instead of having singular values that are growing increasingly smaller, there are two distinct groups of singular values: those that have values between 10^6 and 10^2 and a second set that have a value of $\sim 10^{17}$. The very large singular values are essentially zero in the inverted matrix, since the inverse depends on $\mathbf{\Sigma}^{-1}$. This means that the orthogonal vectors corresponding to these singular values are not incorporated in the solution. Second, the remaining singular values have a much smaller range, which indicates that no subset of orthogonal vectors will overwhelm the solution. In addition, those singular values that contribute to the solution are much different than those chosen in the case of simple truncation. There are values beyond the original truncation point ($\sigma_i | \sim 45 < i < 75$) that are included, allowing for higher-frequency components in the solution to be realized. In addition, there are low-order singular values that are not included (e.g., $\sigma_i | \sim 20$

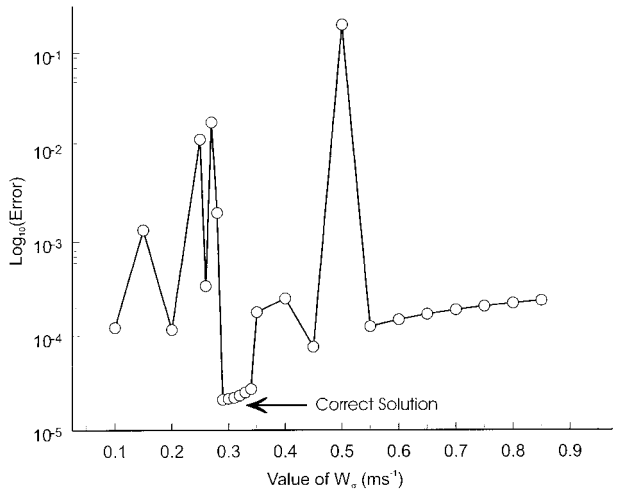

FIG. 7. Plot of the conventional least squares error as a function of turbulent intensity for a simulated spectrum. The spectrum was created using a turbulent intensity of 0.3 m s^{-1} to define the convolution kernel. This value can be correctly retrieved by finding the minimum least squares error, as shown in the graph. The resolution in the neighborhood of the correct solution is increased to show the consistent behavior of the error.

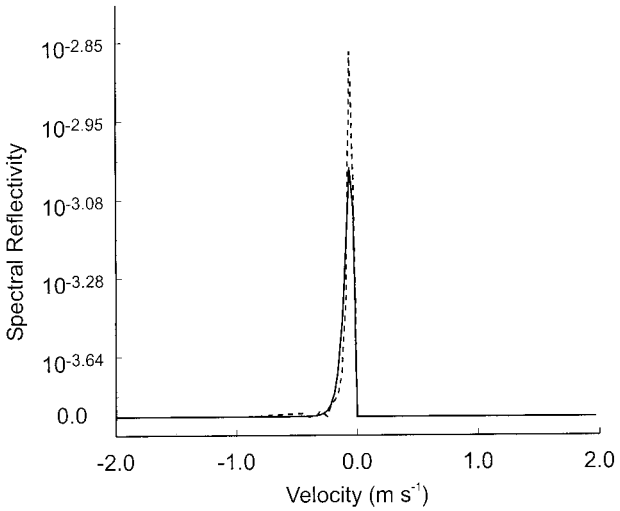

FIG. 9. Retrieved quiet-air spectrum (dashed line) as compared to the original quiet air (solid line).

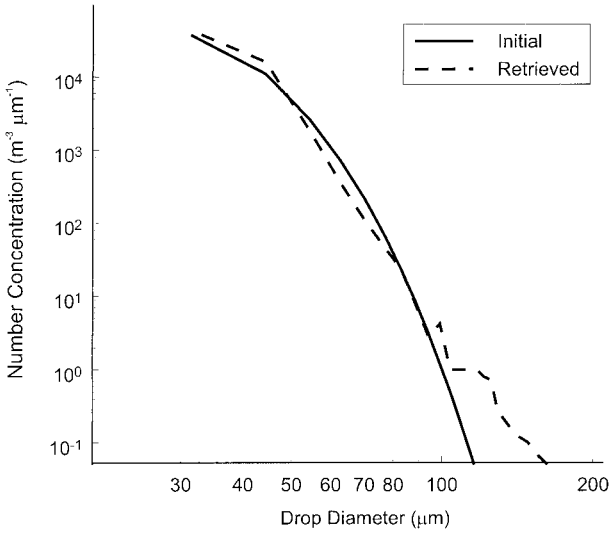

FIG. 10. Comparison of the resulting drop distribution (dashed line) to the original distribution (solid line) used to create the quiet-air spectrum in Fig. 7.

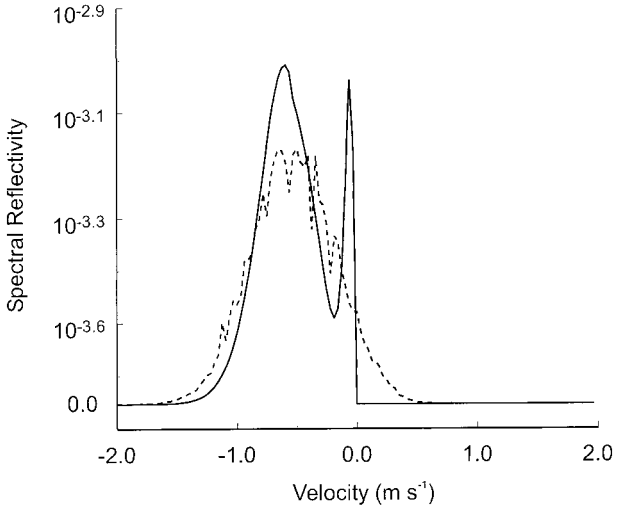

FIG. 11. Same as in Fig. 7 but for a distribution containing both cloud and drizzle modes.

$< i < 25$), which may help reduce the oscillations observed in truncated solutions.

The singular value analysis indicates that the addition of double-sided constraints increases the ability of the inversion to obtain solutions with the correct characteristics. However, in addition to constraining each solution element, we wish to include constraints that deal with the solution set as a whole. One example is an integral equality constraint (e.g., Twomey 1977, p. 160) added to ensure that the integrated reflectivity be conserved through the inversion process. Such constraints are added by the method of LaGrange multipliers. With the added integrated reflectivity constraint, the final solution vector is given by

$$\mathbf{S}_Q = \left[\mathbf{K}^{\mathrm{T}}\mathbf{E}^{-2}\mathbf{K} + \frac{\tau}{n}\mathbf{Q}^{-2}\right]^{-1}\left[\mathbf{K}^{\mathrm{T}}\mathbf{E}^{-2}\mathbf{S}_{\mathrm{meas}} + \frac{\tau}{n}\mathbf{Q}^{-2}\mathbf{d} + \lambda_P\mathbf{1}\right], \tag{10}$$

where $\mathbf{1}$ is an N vector of the form $(1, 1, 1, 1, \ldots)^{\mathrm{T}}$ and λ_p is a LaGrange multiplier having the form

$$\lambda_P = \frac{\sum_{i=1}^{N}[\mathbf{S}_{\mathrm{meas}}(i) - \hat{\mathbf{S}}_Q(i)]}{\sum_{i=1}^{N}\sum_{j=1}^{N}\left[\mathbf{K}^{\mathrm{T}}\mathbf{E}^{-2}\mathbf{K} + \frac{\tau}{n}\mathbf{Q}^{-2}\right]^{-1}_{i,j}}, \tag{11}$$

where $\hat{\mathbf{S}}_Q$ is the unconstrained (without the integral constraint only) solution vector.

The solution described by Eqs. (10) and (11) is straightforward except for the turbulent intensity (w_σ), as defined in Eq. (2). This variable is not only an unknown but is needed to specify the kernel. Therefore, it must be determined prior to the inversion process in order to obtain a correct solution. We found that an acceptable approach to finding the correct value of w_σ was to examine the conventional least squares error over a range of turbulent intensities. This least squares error ρ_0, given by

$$\rho_0 = \min_x(\mathbf{Ax} - \mathbf{p})^{\mathrm{T}}\mathbf{V}^{-2}(\tau)(\mathbf{Ax} - \mathbf{p}), \tag{12}$$

where $\mathbf{x}$ is the solution to Eq. (10), is a minimum at the correct value of w_σ. For example, Fig. 7 shows the least squares error plotted as a function of w_σ for a simulated spectrum. The minimum error occurs very near the correct value of 0.3 m s^{-1}.

The key input to the algorithm is the specification of the constraint envelope as described in Eq. (7). Since the power of the technique resides in the ability to specify the range over which *each* retrieved variable resides, the maximum amount of knowledge about the desired

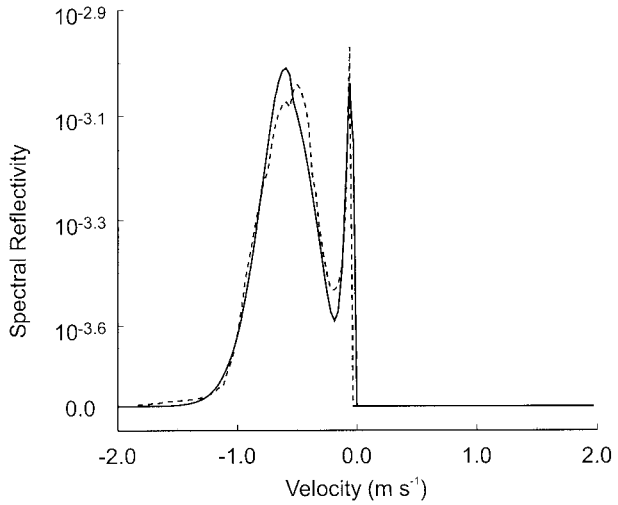

FIG. 12. Same as in Fig. 8 but for the bimodal distribution.

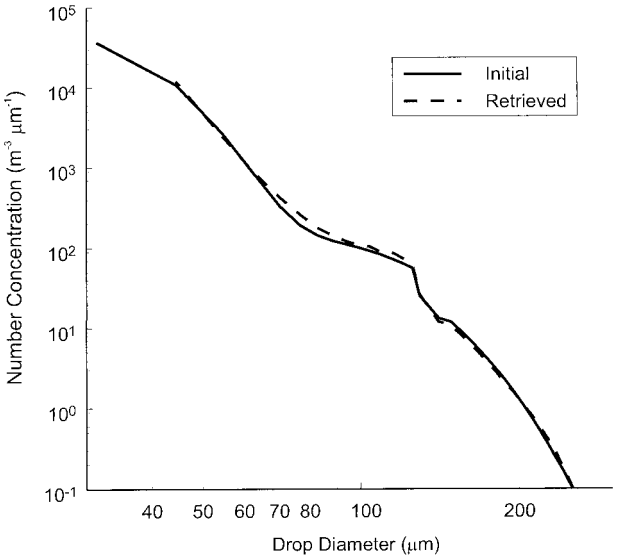

FIG. 13. Comparison of the resulting drop distribution (dashed line) to the original distribution (solid line) used to create the quiet-air spectrum in Fig. 10.

solution should be incorporated into the constraint envelope. This is not to say, however, that we seek to drive the solution to a particular result. Instead, we can incorporate known behavior of convoluted spectra of varying types and degrees of broadening. In the case of operational retrievals, it is thought that these behaviors can be categorized via properties of the measured spectra (e.g., using statistical moments). Furthermore, an iterative process can be used to incorporate a previous solution in order to finetune the final constraint envelope.

3. Algorithm testing

In order to demonstrate the capabilities of the inversion technique, we provide several examples of its use. The algorithm is applied to both simulated data and real observations. This approach to testing allowed us to test the accuracy within a controlled environment and also test the robustness of the algorithm with real data.

a. Simulated spectra

Simulated power spectra were created by convolving a known quiet-air spectrum and specified turbulence distribution via Eq. (3). Each of the quiet-air spectra is generated from a modified gamma distribution of the form

$$N(D)dD = N_M\left(\frac{D}{D_M}\right)^{\alpha} \exp\left[(6+\alpha)\left(1-\frac{D}{D_M}\right)\right]dD, \quad (13)$$

where N_M and D_M are the number concentration and diameter at the maximum spectral reflectivity, respectively, and α is the shape factor. We again emphasize that the technique does not necessitate such an analytical form; this form of a gamma distribution simply facilitates conversion to a radar power spectrum (e.g., Gossard 1994). Multimode drop distributions are created by a linear combination of two or more gamma distributions, each with a set of parameters, N_M, D_M, and α. For each test case, we also calculate more common cloud observables, such as total number concentration (N_T), liquid water content (LWC), and modal diameter (D_o).

The kernel used to create the broadened spectrum is constructed via Eq. (2) with a width of 0.3 m s^{-1}. This width is characteristic of what we have observed in

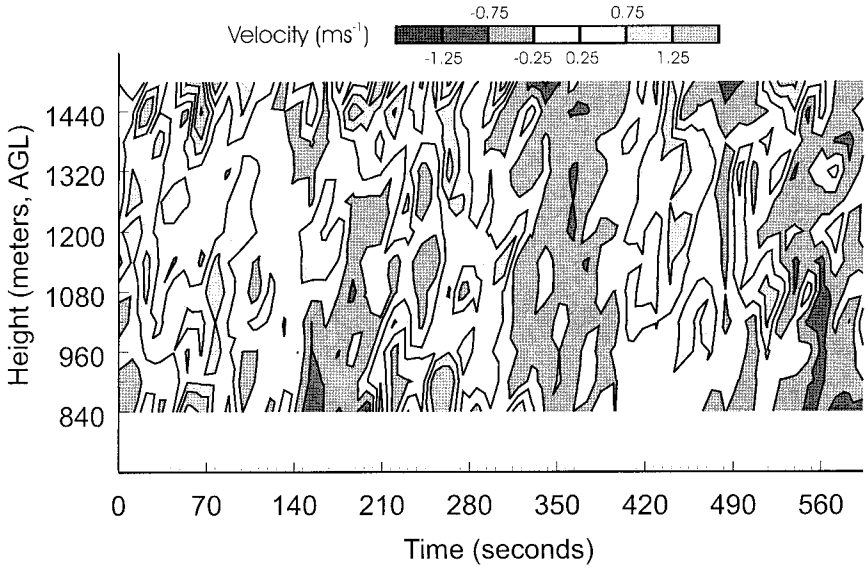

FIG. 14. Contour plot of large-scale vertical velocities within a continental stratocumulus cloud. Contours are drawn every 0.5 m s^{-1}.

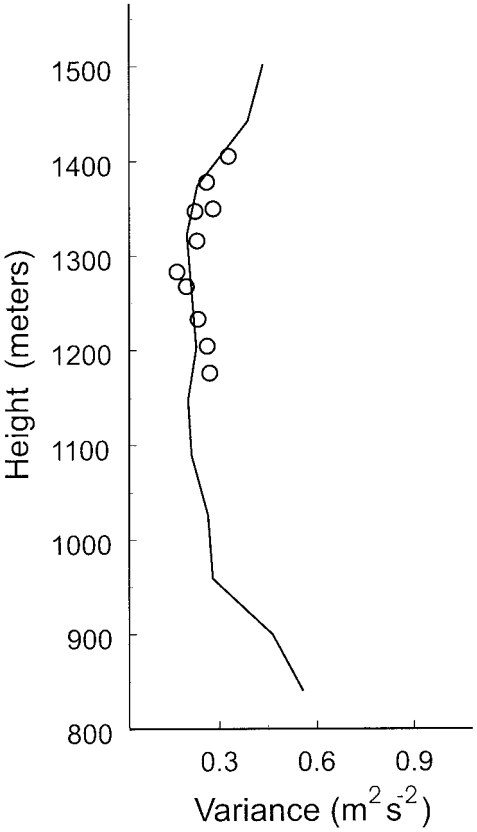

FIG. 15. Profile of radar-derived vertical velocity variance (solid line) compared with aircraft observations of variance (open circles).

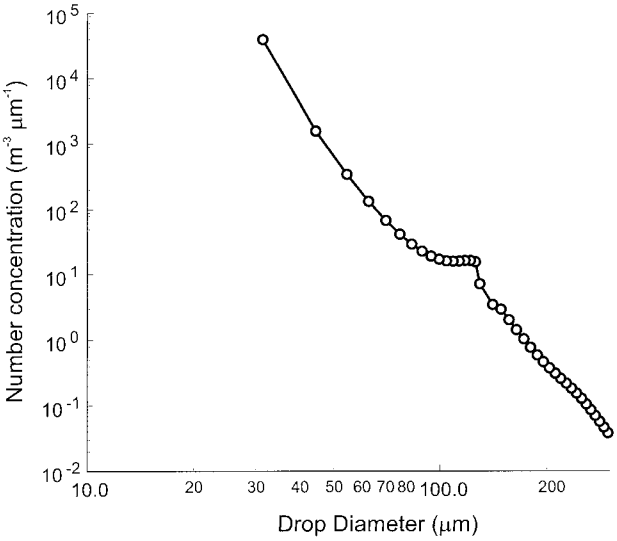

FIG. 16. Retrieved drop distribution from an updraft region of the stratocumulus cloud.

previous studies (Babb et al. 1999). In the retrieval procedure, a Gaussian turbulent kernel is used; however, the width is determined by the routine, using the iterative procedure described in the previous section. Note that although creating a simulated spectrum using the inverse of the equation involved in the retrieval process appears to be less than forthright, this approach would bias results only if the process were completely invertable [i.e., given some process, f, acting on a variable x, one might expect that $f^{-1}(f(x)) = x$]. However, numerical precision is lost both during computation of the forward convolution and the inversion of $\mathbf{K}$ during the deconvolution. This precision loss introduces a measure of noise into the retrieval problem (as demonstrated in the singular value analysis described above). Nevertheless, to ensure that the tests are rigorous, Gaussian distributed noise is added to the simulated spectrum. The added noise is equal to $\mathbf{S}_{\text{meas}}G(\mu = 0, \sigma^2 = 0.4)$, where G is a Gaussian distributed random variable. The value of the standard deviation is similar to the noise characteristics observed in Doppler spectra measured by this radar (although the value varies depending on the signal processing parameters and environmental conditions during the observation). The addition of noise both makes the retrieval more difficult from a numerical standpoint and makes the simulated spectrum resemble what is typically observed.

Tests were designed for several spectra of different forms, especially those having multiple modes that were not easily separable. These types of spectra could not be deconvolved by regression methods, such as those presented by Babb et al. (1999). However, since such spectra make up the majority of those observed, removing turbulence artifacts from these multimode spectra was the prime motivation of this study. Of the many spectra tested, we present two: one having only a small cloud-drop mode and one containing a drizzle mode with little separation from the cloud mode.

The first test case is presented to demonstrate the retrieval of a single, cloud-mode spectrum (Fig. 8). The quiet-air spectrum has a D_M of 40 μm, an N_M of 0.24 cm^3 μm^{-1}, and a shape factor of 3.0 (N_T: 71.3 cm^3; D_o: 13.3 μm; and LWC: 0.39 g m^{-3}). This type of test case was chosen because it resides near the limit of a single-bin quiet-air spectrum. Babb et al. (1999) show that information content in the measured Doppler spectrum about the particle size distribution is decreased with increasing strength of the turbulent wind component relative to the particle fall speed. In cases where only small cloud drops occupy the radar volume, substantial broadening occurs at all bins because even small turbulent vertical velocities are comparable with the terminal fall velocities of all drops.

Despite these difficulties, the retrieval technique performed well. Figure 9 shows that the retrieval algorithm correctly reproduces the quiet-air spectrum shape, including the sharp drop-off at the right-hand edge of the spectrum. Correctly obtaining the right-hand edge of the spectrum is key for removing the large-scale vertical velocity and obtaining a correct measure of the drop distribution. To illustrate the feasibility of retrieving the

drop distribution, the retrieved spectral reflectivity values are converted back to a drop distribution and compared with the original distribution. Figure 10 shows the agreement between the initial and retrieved distributions.

In the second test case shown, we choose a situation where the drizzle mode has an equal maximum spectral reflectivity value compared to the cloud mode. The distribution parameters (D_M, N_M, α) are (a) cloud 40 μm, 0.24 cm^3 μm^{-1}, and 3.0 (same N_T, D_0, LWC as first test) and (b) drizzle 120 μm, 3.3 $\times$ 10^{-4} cm^3 μm^{-1}, and 4.0 (N_T: 0.21 cm^{-3}, D_0: 48.0 μm, LWC: 0.04 g m^{-3}). Figure 11 shows the quiet-air and broadened spectra. Note that the broadened spectrum is dominated by the drizzle signal, with the only indication of the cloud signal being a change of slope at the far right of the spectrum. The retrieval results (Fig. 12) show that the cloud peak can be successfully extracted from the broadened spectrum in addition to the drizzle peak. Examination of the initial and retrieved drop distributions (Fig. 13) show that accurate number concentrations are obtained at all sizes.

These results from simulated spectra show that this algorithm not only performs well in straightforward deconvolutions of single peaks but also in cases where one or more multimode spectral features are indistinguishable due to turbulent broadening. In the following section, we will show how the retrieval technique can be used to assess some of the dynamical and microphysical aspects of a continental stratocumulus cloud.

b. Spectral retrievals in continental stratocumulus

As an example of the technique applied to real data, a liquid-phase continental stratocumulus case was chosen. This cloud persisted over Rock Springs, Pennsylvania, for many hours. Comparisons between radar-derived cloud base and ceilometer cloud base showed indications of drizzle below cloud base, although none was reaching the surface. Spectra were collected at a vertical resolution of 60 m and at a temporal resolution of 8 s. The retrieval algorithm is applied to these spectra in order to demonstrate the types of microphysical and dynamical information that can be obtained from such data.

To demonstrate the dynamical information available via this technique, many consecutive spectral profiles were processed. The large-scale vertical velocity was then extracted from each spectrum by measuring the zero offset of the smallest particles (a good assumption for in-cloud spectra). A section of cloud vertical velocities is shown in Fig. 14. Notice that, as would be expected, the updraft and downdraft regions are distinct features that extend through the depth of the cloud and tend to be slightly sheared. Updrafts tend to be smaller and more intense than their downdraft counterparts. This seems reasonable, since it is likely that the stratocumulus cloud is surface driven.

As a demonstration of profile statistics, Fig. 15 shows the velocity variance as a function of height. Velocity variance from an instrumented aircraft flying in the same cloud is also shown for a smaller height interval. Agreement is good between the two platforms; however, the large temporal resolution difference between the two types of measurements makes such comparisons difficult.

The retrieval of cloud microphysics from radar spectra is more difficult than simply determining the large-scale vertical velocity. A drop size distribution retrieval requires not only that the spectrum be properly deconvolved with the large-scale vertical velocity removed but also an accurate fall-speed versus size relationship based on assumptions about the hydrometeors within the radar volume. In the case of the continental stratocumulus cloud, we are confident that the cloud contained only liquid drops. Therefore, we used the size versus fall-speed relationship that Babb et al. (1999) use, namely, a quadratic function of drop diameter for drops within the Stokes range and a linear function of diameter for larger drops. Figure 16 shows a drop distribution retrieved in an updraft region of the stratocumulus cloud. Although the values seem reasonable, it is difficult to verify such an individual drop distribution. It is likely that statistics describing the drop distribution (e.g., mean diameter, liquid water, etc.) will need to be compared with similar statistics from aircraft observations.

4. Summary and conclusions

In this paper, a technique was developed to remove the turbulent broadening of observed radar Doppler power spectra collected at vertical incidence. The algorithm employed is noteworthy in that no assumptions concerning the drop distribution are required. The approach centers on the linearization of the convolution between the turbulent air motions and the quiet-air Doppler spectrum. The resulting system of equations are then inverted to solve for the unknown quiet-air spectrum.

However, as in most remote sensing applications, the kernel matrix to be inverted is nearly singular, and thus, its inversion is unstable, resulting in the amplification of measurement and computational uncertainties. Successful techniques to circumvent this error amplification have focused on adding constraints to the solution. Each constraint specifies how a particular variable in the solution is to act or how many variables respond to each other. Adding constraints guides the outcome of the inversion, and thus reduces the solution space (which is large in unstable problems) as a whole. However, many constraints tend to be too loose (i.e., only bounding one aspect of the desired solution), while others tend to be too restrictive (i.e., driving the solution toward a particular, sometimes parametric, solution).

For our problem, we have adapted a technique found

in the literature of related disciplines that uses double-sided constraints on each unknown variable. The advantage of such a technique is that each variable's constraint interval can be adjusted according to the amount of knowledge available concerning the solution of that particular variable. This inversion algorithm was tested on both simulated and real data. Tests performed on simulated data determined the behavior of the algorithm in a controlled environment, while tests on large volumes of real data established the technique's robustness.

Observed Doppler spectra were simulated using known dropsize and vertical air motion distributions. Gaussian-distributed random noise was also added to the broadened Doppler spectra in order to produce realistic test cases. The simulated spectrum was used as input to the retrieval algorithm, and the result was compared to the initial quiet-air spectrum. Of the numerous spectra tested in this manner, two tests representing various retrieval challenges are presented. Each case illustrates a physical situation where information about the quiet-air spectrum is lost due to the effects of turbulence. They include masking of the cloud signal by a highly reflective drizzle mode and a single, narrow cloud mode spectrum. Results from the two cases indicate that accurate retrievals can be performed despite the addition of moderate amounts of noise to the simulated spectra. Furthermore, comparison of the initial and retrieved drop size distributions show considerable agreement. These tests demonstrate that both cloud microphysics and dynamics (i.e., large-scale vertical velocity and subvolume scale turbulent intensity) can, in principle, be retrieved from turbulent broadened spectra.

To demonstrate the practical retrieval of these quantities, the algorithm was used to process Doppler spectra collected during a continental stratocumulus experiment in Pennsylvania. From these spectra, an x–z depiction of the large-scale vertical motions within the cloud was constructed. This slice showed coherent updraft and downdraft structures throughout the depth of the cloud. Also shown was a profile of vertical velocity variance, which agreed well with aircraft measurements. To demonstrate microphysical retrieval, a drop size distribution was shown from an updraft region of the cloud. Although the values seem reasonable, it is yet unclear how such an individual retrieval might be verified. It is suggested that obtaining a correlated set of statistics between aircraft and the radar may provide a suitable argument for retrieval accuracy. It also should be noted that for the best drop distribution retrievals, minimizing the velocity resolution of each spectrum is key (as opposed to minimizing the temporal resolution between spectra for dynamics). As the velocity bin width is decreased, the smaller diameter drops can be resolved.

This technique is a major improvement over parametric retrievals, such as those presented by Babb et al. (1999). With their method, the turbulence effect on an analytical drop distribution is modeled by a parametric equation having three unknowns, which are found by a least squares fit to the data. One major drawback to this approach is that assumptions concerning the cloud drop size distribution must be made *before* the turbulence effects are accounted for. The goal of the current approach is to remove the turbulence effects first, making no assumptions about the cloud properties, *then* making the appropriate assumptions to retrieve the cloud microphysics and dynamics. This methodology is especially important when dealing with ice or mixed-phase clouds. Currently, this technique is being applied to lake-effect snow squalls, with excellent results retrieving the cloud-scale dynamics. Future work is planned to match spectral features in the retrieved quiet-air spectra with different phases/habits of cloud particles.

Acknowledgments. We wish to gratefully acknowledge the contributions of Chris Ruff, Natasha Miles, and the reviewers who greatly improved the paper. This work was partially funded by grants from NSF (ATM9873643) and DOE (DE-F602-90ER61071).

REFERENCES

Babb, D. M., J. Verlinde, and B. A. Albrecht, 1999: Retrieval of cloud microphysical parameters from 94-GHz radar Doppler power spectra. *J. Atmos. Oceanic Technol.,* **16,** 489–503.

Battan, L. J., 1964: Some observations of vertical velocities and precipitation sizes in a thunderstorm. *J. Appl. Meteor.,* **3,** 415–493.

Boot, J. C. G., 1964: *Quadratic Programming: Algorithms, Anomalies [and] Applications.* North-Holland Publishing Company and Rand McNally and Company, 213 pp.

Boyenval, E. H., 1960: Echoes from precipitation using pulsed Doppler radar. *Proc. Eight Weather Radar Conf.,* San Francisco, CA, Amer. Meteor. Soc., 57–64.

Dubovik O. V., T. V. Lapyonok, and S. L. Oshchepkov, 1995: Improved technique for data inversion: Optical sizing of multicomponent aerosols. *Appl. Opt.,* **34,** 8422–8436.

Fukao, S., K. Wakasugi, T. Sato, S. Morimoto, T. Tsuda, I. Hirota, I. Kimura, and S. Kato, 1985: Direct measurements of air and precipitation particle motion by VHF Doppler radar. *Nature,* **316,** 712–714.

Golub, G., and W. Kahan, 1965: Calculating the singular values and pseudo-inverse of a matrix. *SIAM J. Numer. Anal.,* **2b,** 205–224.

Gossard, E. E., 1988: Measuring drop size distributions in cloud with clear-air sensing Doppler radar. *J. Atmos. Oceanic Technol.,* **5,** 640–649.

——, 1994: Measurement of cloud droplet spectra by Doppler radar. *J. Atmos. Oceanic Technol.,* **11,** 712–726.

——, and R. G. Strauch, 1989: Further guide for the retrieval of dropsize distributions in water clouds with a ground-based clear-air-sensing Doppler radar. NOAA/ERL/Wave Propagation Laboratory Tech. Document, 48 pp.

——, ——, and R. R. Rogers, 1990: Evolution of dropsize distributions in liquid precipitation observed by ground-based Doppler radar. *J. Atmos. Oceanic Technol.,* **7,** 815–828.

——, J. B. Snider, E. E. Clothiaux, B. Martner, J. S. Gibson, R. A. Kropfli, and A. S. Frisch, 1997: The potential of 8-mm radars for remotely sensing cloud drop size distributions. *J. Atmos. Oceanic Technol.,* **14,** 76–87.

Hauser, D., and P. Amayenc, 1981: A new method for deducing hydrometeor-size distributions and vertical air motions from Doppler radar measurements at vertical incidence. *J. Appl. Meteor.,* **20,** 547–555.

——, and ——, 1983: Exponential size distributions of raindrops and

vertical air motions deduced from vertically pointing Doppler radar using a new method. *J. Climate Appl. Meteor.,* **22,** 407–418.

Lawson, C. L., and R. J. Hanson, 1974: *Solving Least Squares Problems.* Prentice-Hall Inc., 340 pp.

Lhermitte, R. M., 1960: The use of special ''pulse Doppler radar'' in measurements of particle fall velocities. *Proc. Eigth Weather Radar Conf.,* San Francisco, CA, Amer. Meteor. Soc., 269–275.

Miles, N. L., J. Verlinde, and E. E. Clothiaux, 2000: Cloud droplet size distributions in low-level stratiform clouds. *J. Atmos. Sci.,* **57,** 295–311.

Pierce, J. E., and B. W. Rust, 1985: Constrained least squares interval estimation. *SIAM J. Sci. Stat. Comput.,* **6,** 670–683.

Radke, L. F., J. A. Coakley Jr., and M. D. King, 1989: Direct and remote sensing observations of the effects of ships on clouds. *Science,* **246,** 1146–1149.

Rogers, C. D., 1976: Retrieval of atmospheric temperature and composition from remote measurements of thermal radiation. *Rev. Geophys. Space Phys.,* **14,** 609–624.

Rogers, R. R., 1964: An extension of the *Z–R* relation for Doppler radar. *Proc. World Conf. on Radio Meteorology and 11th Weather Radar Conf.,* Boulder, CO, Amer. Meteor. Soc., 158–161.

——, and R. J. Pilie, 1962: Radar measurements of drop-size distributions. *J. Atmos. Sci.,* **19,** 503–508.

Rust, B. W., 1998: Truncating the singular value decomposition for ill-posed problems. National Institute of Standards and Technology, Tech. Rep. 6131, U.S. Department of Commerce, 33 pp. [Available from NIST, Applied and Computational Mathematics Division, Gaithersburg, MD 20899.]

——, and D. P. O'Leary, 1994: Confidence intervals for discrete approximations to ill-posed problems. *J. Comput. Graph. Stat.,* **3,** 67–96.

Stevens, G. L., and P. J. Webster, 1979: Sensitivity of radiative forcing to variable cloud and moisture. *J. Atmos. Sci.,* **36,** 1542–1553.

Stokes, G. M., and S. E. Schwartz, 1994: The Atmospheric Radiation Measurement (ARM) Program: Programmatic background and design of the cloud and radiation test bed. *Bull. Amer. Meteor. Soc.,* **75,** 1201–1221.

Twomey, S., 1977: *Introduction to the Mathematics of Inversion in Remote Sensing and Indirect Measurements.* Dover Publications Inc., 243 pp.

Wakasugi, K., S. Fukao, S. Kato, A. Mizutani, and M. Matsuo, 1985: Air and precipitation particle motions within a cold front measured by the MU VHF radar. *Radio Sci.,* **20,** 1233–1240.

——, A. Mizutani, M. Matsuo, S. Fukao, and S. Kato, 1987: Further discussion on deriving dropsize distribution and vertical air velocities directly from VHF Doppler radar spectra. *J. Atmos. Oceanic Technol.,* **4,** 170–179.